Subgenual Anterior Cingulate Cortex Functional Connectivity Abnormalities in Depression: Insights from Brain Imaging Big Data and Precision-Guided Personalized Intervention via Transcranial Magnetic Stimulation

Xiao Chen[1,2,3,4,5]#, Bin Lu[1,3,4,5]#, Yu-Wei Wang[1,3,4,5], Xue-Ying Li[1,3,4,5], Zi-Han Wang[1,3,4,5], Hui-Xian Li[6], Yi-Fan Liao[1,3,4,5], Daniel M. Blumberger[2,7], Francisco Xavier Castellanos[8,9], Eduardo A. Garza-Villarreal[10], Li-Ping Cao[11], Guan-Mao Chen[12], Jian-Shan Chen[11], Tao Chen[13], Tao-Lin Chen[14,15], Yan-Rong Chen[1,3,4,5], Yu-Qi Cheng[16], Zhao-Song Chu[16], Shi-Xian Cui[1,17,18], Xi-Long Cui[19], Zhao-Yu Deng[1,3,4,5], Qing-Lin Gao[1,3,4,5], Qi-Yong Gong[14,15], Wen-Bin Guo[19], Can-Can He[20], Zheng-Jia-Yi Hu[1,17,18], Qian Huang[21], Xin-Lei Ji[19], Feng-Nan Jia[22], Li Kuang[21], Bao-Juan Li[23], Feng Li[24], Tao Li[25,26], Xue Li[1,3,4,5], Tao Lian[1,3,4,5], Xiao-Yun Liu[27], Yan-Song Liu[22], Zhe-Ning Liu[19], Yi-Cheng Long[19], Jian-Ping Lu[28], Jiang Qiu[29], Xiao-Xiao Shan[19], Tian-Mei Si[30], Peng-Feng Sun[31], Chuan-Yue Wang[24], Han-Lin Wang[1,3,4,5], Xiang Wang[19], Ying Wang[12], Chen-Nan Wu[1,3,4,5], Xiao-Ping Wu[31], Xin-Ran Wu[29], Yan-Kun Wu[30], Chun-Ming Xie[20], Guang-Rong Xie[19], Peng Xie[32,33,34], Xiu-Feng Xu[16], Zhen-Peng Xue[28], Hong Yang[13], Jian Yang[33], Hua Yu[25,26], Yong-Qiang Yu[35,36,37], Min-Lan Yuan[38], Yong-Gui Yuan[27], Yu-Feng Zang[39,40], Ai-Xia Zhang[41], Ke-Rang Zhang[41], Wei Zhang[38], Zi-Jing Zhang[1,3,4,5], Jing-Ping Zhao[19], Jia-Jia Zhu[35,36,37], Xi-Nian Zuo[42,43], the DIRECT Consortium, Hua-Ning Wang[23], Chao-Gan Yan[1,3,4,5,17,18]*

[1]CAS Key Laboratory of Behavioral Science, Institute of Psychology, Beijing 100101, China

[2]Temerty Centre for Therapeutic Brain Intervention, Campbell Family Research Institute, Centre for Addiction and Mental Health, Toronto, Ontario M6J1H4, Canada

[3]Magnetic Resonance Imaging Research Center, Institute of Psychology, Chinese Academy of Sciences, Beijing 100101, China

[4]Department of Psychology, University of Chinese Academy of Sciences, Beijing 100049, China

[5]International Big-Data Center for Depression Research, Chinese Academy of Sciences, Beijing 100101, China

[6]The Third Affiliated Hospital of Zhengzhou University, Zhengzhou, Henan 450052, China

[7]Department of Psychiatry, Temerty Faculty of Medicine, University of Toronto, Toronto, Ontario

M5S1A1, Canada

[8]Department of Child and Adolescent Psychiatry, NYU Grossman School of Medicine, New York, NY 10016, USA

[9]Nathan Kline Institute for Psychiatric Research, Orangeburg, NY 10962, USA

[10]Instituto de Neurobiologia, Universidad Nacional Autonoma de Mexico camus Juriquilla, Queretaro 7630, Mexico

[11]Affiliated Brain Hospital of Guangzhou Medical University, Guangzhou, Guangdong 510370, China

[12]The First Affiliated Hospital of Jinan University, Guangzhou, Guangdong 250024, China

[13]Department of Radiology, The First Affiliated Hospital, College of Medicine, Zhejiang University, Hangzhou, Zhejiang 310058, China

[14]Department of Radiology and Huaxi MR Research Center (HMRRC), Functional and Molecular Imaging Key Laboratory of Sichuan Province, West China Hospital of Sichuan University, Chengdu, Sichuan 610041, China

[15]Research Unit of Psychoradiology, Chinese Academy of Medical Sciences, Chengdu, Sichuan 610041, China

[16]Department of Psychiatry, First Affiliated Hospital of Kunming Medical University, Kunming, Yunnan 650032, China

[17]Sino-Danish College, University of Chinese Academy of Sciences, Beijing 101408, China

[18]Sino-Danish Center for Education and Research, Graduate University of Chinese Academy of Sciences, Beijing 101408, China

[19]Department of Psychiatry, and National Clinical Research Center for Mental Disorders, The Second Xiangya Hospital of Central South University, Changsha, Hunan 410011, China

[20]Department of Neurology, Affiliated ZhongDa Hospital of Southeast University, Nanjing, Jiangsu 210009, China

[21]Department of Psychiatry, The First Affiliated Hospital of Chongqing Medical University, Chongqing 400042, China

[22]Department of Clinical Psychology, Suzhou Psychiatric Hospital, The Affiliated Guangji Hospital of Soochow University, Suzhou, Jiangsu 215003, China

[23]Xijing Hospital of Air Force Military Medical University, Xi'an, Shaanxi 710032, China

[24]Beijing Anding Hospital, Capital Medical University, Beijing 100120, China

[25]Affiliated Mental Health Center & Hangzhou Seventh People's Hospital, Zhejiang University School of Medicine, Hangzhou, Zhejiang 310063, China

[26]Mental Health Center and Psychiatric Laboratory, West China Hospital of Sichuan University, Chengdu, Sichuan 610044, China

[27]Department of Psychosomatics and Psychiatry, Zhongda Hospital, School of Medicine, Southeast University, Nanjing, Jiangsu 210009, China

[28]Shenzhen Kangning Hospital, Shenzhen, Guangzhou 518020, China

[29]Faculty of Psychology, Southwest University, Chongqing 400715, China

[30]National Clinical Research Center for Mental Disorders (Peking University Sixth Hospital) & Key Laboratory of Mental Health, Ministry of Health (Peking University), Beijing 100191, China

[31]Xi'an Central Hospital, Xi'an, Shaanxi 710004, China

[32]Institute of Neuroscience, Chongqing Medical University, Chongqing 400016, China

[33]Chongqing Key Laboratory of Neurobiology, Chongqing 400000, China

[34]Department of Neurology, The First Affiliated Hospital of Chongqing Medical University, Chongqing 400042, China

[35]Department of Radiology, The First Affiliated Hospital of Anhui Medical University, Hefei, Anhui 230022, China

[36]Research Center of Clinical Medical Imaging, Hefei, Anhui 230032, China

[37]Anhui Provincial Institute of Translational Medicine, Hefei, Anhui 230032, China

[38]West China Hospital of Sichuan University, Chengdu, Sichuan 610044, China

[39]Center for Cognition and Brain Disorders, The Affiliated Hospital of Hangzhou Normal University, Hangzhou, Zhejiang 310018, China

[40]Zhejiang Key Laboratory for Research in Assessment of Cognitive Impairments, Hangzhou, Zhejiang 310000, China

[41]First Hospital of Shanxi Medical University, Taiyuan, Shanxi 030001, China

[42]Developmental Population Neuroscience Research Center, IDG/McGovern Institute for Brain Research, Beijing Normal University, Beijing 100091, China

[43]National Basic Science Data Center, Beijing 100038, China

[44]Department of Psychiatry, Sir Run Run Shaw Hospital, Zhejiang University School of Medicine, Hangzhou, Zhejiang 310020, China

[45]Shanghai Mental Health Center, Shanghai Jiao Tong University School of Medicine, Shanghai 200030, China

[46]Department of Diagnostics, Affiliated Hospital, Hangzhou Normal University Medical School, Hangzhou, Zhejiang 311121, China

[47]Department of Psychiatry, First Affiliated Hospital, China Medical University, Shenyang, Liaoning 110122, China

[48]Early Intervention Unit, Department of Psychiatry, Affiliated Nanjing Brain Hospital, Nanjing Medical University, Nanjing, Jiangsu 210024, China

[49]Department of Neurology, The First Affiliated Hospital of Anhui Medical University, Hefei, Anhui 230022, China

[50]Department of Psychiatry, Shanghai Jiao Tong University School of Medicine, Shanghai 200025, China

*Corresponding author:

Chao-Gan Yan, Ph. D.

CAS Key Laboratory of Behavioral Science, Institute of Psychology, Beijing, China

16 Lincui Road, Chaoyang District, Beijing 100101, China

Tel: +86-10-64101582

E-mail: yancg@psych.ac.cn

#Xiao Chen and Bin Lu contributed equally to this work.

DIRECT consortium: Chao-Gan Yan, Ph.D.[1,3,4,5,17,18], Xiao Chen, Ph.D.[1,2,3,4,5], Li-Ping Cao, M.D.[11], Wei Chen, M.D.[44], Yu-Qi Cheng, M.D.[16], Yi-Ru Fang, M.D.[45], Qi-Yong Gong, M.D.[14,15], Wen-Bin Guo, M.D.[19], Li Kuang, M.D.[21], Bao-Juan Li, M.D.[23], Tao Li, M.D.[25,26], Yan-Song Liu, M.D.[22], Zhe-Ning Liu, M.D.[19], Jian-Ping Lu, M.D.[28], Qing-Hua Luo, M.D.[21], Hua-Qing Meng, M.D.[21], Dai-Hui Peng, M.D.[45], Jiang Qiu, Ph.D.[29], Yue-Di Shen, M.D.[46], Tian-Mei Si, M.D.[30], Yan-Qing Tang, M.D.[47], Chuan-Yue Wang, M.D.[24], Fei Wang, M.D.[47,48], Hua-Ning Wang, M.D.[23], Kai Wang, M.D.[49], Xiang Wang, M.D.[19], Ying Wang, M.D.[12], Xiao-Ping Wu, M.D.[31], Chun-Ming Xie, M.D.[20], Guang-Rong Xie, M.D.[19], Peng Xie, M.D.[32,33,34], Xiu-Feng

115 Xu, M.D.[16], Hong Yang, M.D.[13], Jian Yang, M.D.[33], Shu-Qiao Yao, M.D.[19], Yong-Qiang Yu, M.D.[35,36,37],

116 Yong-Gui Yuan, M.D.[27], Ke-Rang Zhang, M.D.[41], Wei Zhang, M.D.[38], Zhi-Jun Zhang, M.D.[20], Jun-Juan Zhu,

117 M.D.[50], Xi-Nian Zuo, Ph.D.[42,43], Jing-Ping Zhao, M.D.[19], Yu-Feng Zang, M.D.[39,40]

Abstract

Background The subgenual anterior cingulate cortex (sgACC) plays a central role in the pathophysiology of major depressive disorder (MDD), and its functional interactive profile with the left dorsal lateral prefrontal cortex (DLPFC) is associated with transcranial magnetic stimulation (TMS) treatment outcomes. Nevertheless, previous research on sgACC functional connectivity (FC) in MDD has yielded inconsistent results, partly due to small sample sizes and limited statistical power. Furthermore, calculating sgACC-FC to target TMS individually is challenging.

Methods Leveraging a large multi-site cross-sectional sample (1660 MDD patients vs. 1341 healthy controls) from Phase II of the Depression Imaging REsearch ConsorTium (DIRECT), we systematically delineated case-control difference maps of sgACC-FC. Then, we explored the potential impact of such group-level abnormality profiles on the TMS target localization and clinical efficacy. Next, we developed an MDD big data-guided individualized TMS targeting algorithm to integrate group-level statistical maps with individual-level brain activity to localize TMS targets individually.

Results We found an enhanced sgACC-DLPFC FC in MDD patients compared to healthy controls (HC). Such group differences altered the position of the sgACC anti-correlation peak in the left DLPFC. In two independent clinical samples, we showed that the magnitude of TMS targets' case-control differences in sgACC FC was related to clinical improvement. The MDD big data-guided individualized TMS targeting algorithm may generate individualized TMS targets that are clinically superior to group-level targets.

Interpretation We reliably delineated MDD-related abnormalities of sgACC-FC profiles in a large, independently ascertained sample and demonstrated the potential impact of such case-control differences on FC-guided localization of TMS targets.

Funding Ministry of Science and Technology of the People's Republic of China, National Natural Science Foundation of China, and Chinese Academy of Sciences

Keywords: major depressive disorder, transcranial magnetic stimulation, individualization, subgenual anterior cingulate cortex, functional connectivity, dual regression

146

Introduction

Major depressive disorder (MDD) is a common and debilitating psychiatric disorder projected to be the most burdensome condition worldwide by 2030 [1]. Despite extensive research, the pathophysiology of MDD remains elusive. Nevertheless, a key putative brain region or network hub appears to be the subgenual anterior cingulate cortex (sgACC), which shows reproducible metabolic hyperactivity [2], has been implicated in emotional responses, motivation, and rumination in MDD [3], and it has been shown to be an important target in deep brain stimulation and transcranial magnetic stimulation (TMS) [4,5]. Repetitive TMS above 5 Hz on the left dorsolateral prefrontal cortex (DLPFC) indirectly stimulates the sgACC, and the closer to the sgACC target, the better the clinical outcome [6]. Accordingly, identifying an optimized neuromodulation target in the left DLPFC based on sgACC-related functional connectivity (FC) is crucial for developing effective depression treatments [7,8]. In light of inconsistent findings derived from studies with small sample sizes [9-15], we set out to establish a large sample to identify a reliable abnormal sgACC-DLPFC FC profile in MDD and further integrate this profile with individual brain activity to generate individualized neuromodulation targets for treating depression.

Numerous investigations have delved into FC abnormalities in MDD using resting-state functional magnetic resonance imaging (R-fMRI). Abnormal FCs between sgACC and amygdala, thalamus, temporal gyrus, lingual gyrus, cerebellum, DLPFC, and default mode network (DMN) regions such as medial and dorsal medial prefrontal cortex, precuneus, and parahippocampus have been reported [9,10,13-20]. However, findings have been inconsistent, making integrating findings and generating precise profiles of sgACC-related FC abnormalities challenging. This deficiency in reproducibility could be partially due to small sample sizes, differences in preprocessing pipelines, and low statistical power of clinical imaging studies [21,22]. To address the issue of limited sample size, we initiated the Depression Imaging REsearch ConsorTium (DIRECT) [23] and conducted an initial meta/mega-analysis (N_{MDD} = 1300), referred to as REST-meta-MDD [24]. DIRECT Phase I shared ROI-level signals, thus enabling the

175 investigation of multiple MDD-related abnormalities in network FC, FC topological and
176 dynamic features, and functional lateralization [24-31]. In DIRECT Phase II data reporting, we
177 pooled an expanded MDD sample (N_{MDD} = 1660), which was preprocessed with a
178 surface-based pipeline, DPABISurf [32]. DIRECT Phase II shared voxel/vertex level BOLD time
179 series, allowing more flexible and thorough investigations. Leveraging the most
180 comprehensive MDD R-fMRI dataset to date encompassing depression patients and healthy
181 controls, we can determine an aberrant sgACC-FC profile associated with MDD, characterized
182 by superior reproducibility and low risk of false positives.
183
184 Maps of sgACC-related FC abnormalities are clinically useful for predicting repetitive TMS
185 (rTMS) treatment outcomes in MDD patients [33-35]. Specifically, the anti-correlation between
186 sgACC and left DLPFC has been associated with clinical improvement from rTMS treatment
187 [36-40]. This has led to the intriguing notion that the FC between sgACC and left DLPFC could be
188 leveraged to identify more precise rTMS targets and improve the efficacy of rTMS delivered
189 to the left DLPFC [7,41]. Researchers have identified a group-wise TMS target [38], which was the
190 most anticorrelated DLPFC site to sgACC in the mean FC map from a large cohort of healthy
191 adults. Subtle but significant case-control differences in resting-state FC profiles have been
192 identified in a large sample of MDD patients [24]. Thus, understanding the profiles of sgACC FC
193 case-control differences and their impact on potential targets for rTMS applied to the left
194 DLPFC could be a critical step toward developing optimized rTMS target site identification
195 methods.
196
197 Individual human brains exhibit highly heterogeneous functional organization [42], with the
198 DLPFC regions exhibiting the highest level of interindividual variation in cytoarchitecture,
199 brain function, and network connectivity profiles [8,43]. While several individualized FC-guided
200 TMS target identification algorithms have been proposed [36,41,44-48], the target localizations of
201 most existing TMS protocols have not been individualized. The major obstacles to identifying
202 individualized TMS locations are the low signal-to-noise ratio in the sgACC area and the poor
203 reproducibility of individual FC maps [49,50]. The high reliability and statistical power of the

DIRECT MDD cohort (N_{MDD} = 1660) allow the integration of group-level statistical maps and individual functional brain images to achieve precise and reliable TMS localization. Here, we propose an MDD big data-guided individualized TMS targeting algorithm based on dual regression (DR), which was initially developed for mapping group-level independent component analysis (ICA) results onto individual brains [51]. During individualized target localization, the DR calculation is entirely confined to the DLPFC region, which has a high signal-to-noise ratio, avoiding noisy signals from the sgACC region. Thus, this approach enhances the efficacy and reliability of individualization approaches for identifying TMS targets [52].

In the present study, we leverage a large-scale multi-center sample (DIRECT Phase II, 1660 MDD patients and 1341 healthy controls (HCs)) to derive a reliable sgACC-related FC abnormality profile for MDD. Next, we showed that such case-control difference profiles may be related to the clinical efficiency of TMS and that the positions of the sgACC anti-correlation peaks might be different in the MDD patients as compared to the HCs. In light of this, we developed an MDD big data-guided individualized TMS targeting algorithm that may boost the clinical efficiency of TMS. We hypothesized that MDD patients would show a significantly abnormal sgACC-FC profile, especially in the left DLPFC. We also hypothesized that our newly developed DR-based approach would outperform traditional TMS group targets. To our knowledge, this is the first study to show the possible implications of the case-control abnormalities regarding the sgACC-FC profiles on the TMS target localization and to integrate large-scale group-level statistical maps with individual-level spontaneous brain activity to achieve individualized TMS targeting in MDD.

Materials and methods

Study sample

This study utilized four independent datasets. The first dataset (“DIRECT”) is a large-scale,

multi-site consortium sharing standardized preprocessed R-fMRI time series. Building on the initial success of DIRECT Phase I (the REST-meta-MDD Project) [24], consortium members and international collaborators met on May 11th-12th, 2019, and agreed to launch DIRECT Phase II, which comprises 23 case-control designed datasets, including R-fMRI and T1 structural scans from 1660 MDD patients and 1341 HCs. Researchers from each site took a 2-day DPABISurf training course on September 14th-15th, 2019, to harmonize the organization and preprocessing of R-fMRI/T1 structural data. Demographic and clinical characteristics for each sample are presented in Figure 1 and Table 1. Site information, sample size, and previous publications based on the shared data are listed in Table S1. All participants were asked to self-report their sex (biological attribute) as part of the case report form (CRF). All participants in DIRECT Phase II were East Asian. Patients were diagnosed with MDD based on ICD 10 or DSM-IV. Healthy controls matched with MDD patients by age, sex ratio, and educational levels were recruited at each site. All participants provided written informed consent, and local institutional review boards approved each study from all included cohorts. The analysis plan of the current study has been reviewed and approved by the Institutional Review Board of the Institute of Psychology, Chinese Academy of Sciences (No. H21102). Data will be made available to the public as outlined in the Data Sharing Statement.

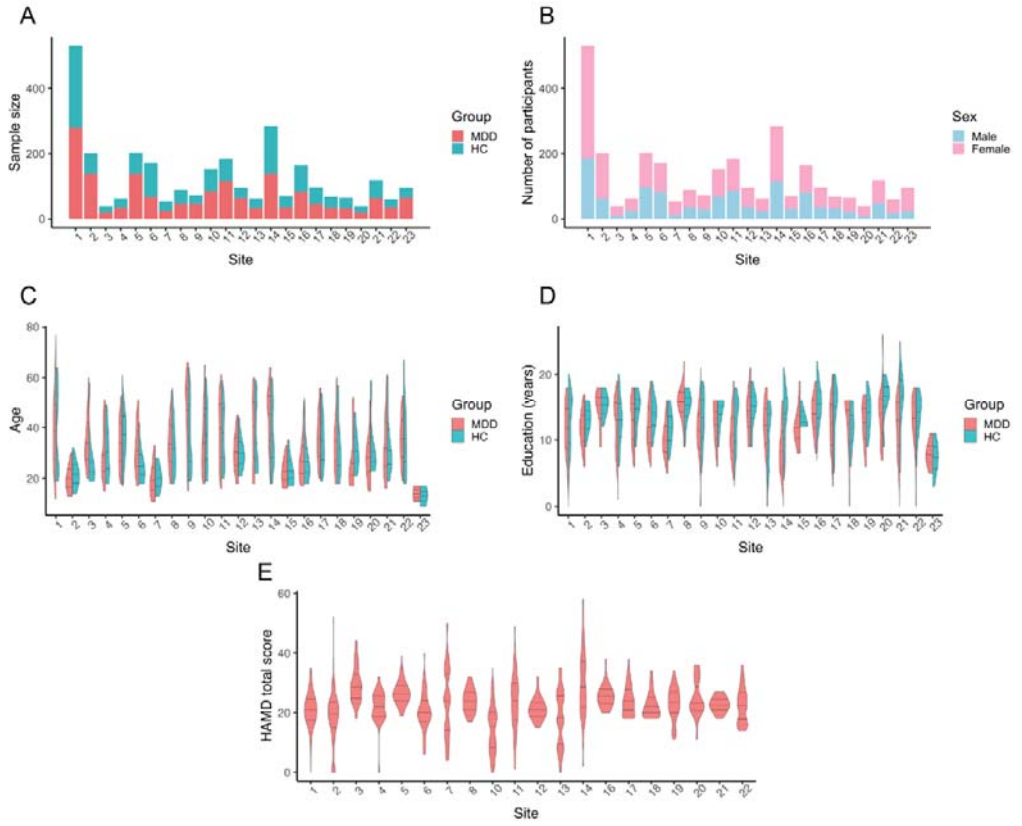

Figure 1. Sample characteristics of the DIRECT dataset. (A) Sample sizes of each site; (B) Number of male/female subjects irrespective of diagnosis; (C) Violin plots depicting the age distribution (in years). Solid black lines indicate the mean, 25th, and 75th percentiles; (D) Violin plots show education distribution (in years). Solid black lines indicate the mean, 25th, and 75th percentiles; (E) Violin plots depicting the distribution of scores of the Hamilton Depression Rating Scale (HAMD). Solid black lines indicate the mean, 25th, and 75th percentiles.

The second dataset ("TRD-TMS") comprises 25 medication-treatment-resistant MDD (TRD) patients who underwent 4 to 7 weeks of daily repetitive TMS applied over the left DLPFC. Patients' TMS sites were recorded using their structural MRI images and a frameless neuronavigation system. Treatment response was assessed with the 24-item Hamilton Depression Rating Scale (HAMD). The targets for rTMS stimulation were determined using the 5.5-cm method. Only TMS outcomes and target coordinates were openly shared for this

dataset. We obtained access to these data from the supplementary materials of Weigand et al. [38]. For more details on this dataset, please refer to Weigand et al. [38].

The third dataset ("SID-TMS") consists of 28 MDD patients with suicidal ideation who underwent 10 daily sessions of rTMS over the left DLPFC for 5 consecutive days. Clinical efficacy was evaluated using a 17-item HAMD. The TMS outcomes, neuroimaging data, participants' demographic information, and target coordinates for this dataset were made available upon request, enabling evaluation of the performance of the MDD big data-guided individualized TMS targeting algorithm. The targets for individualized rTMS stimulation were determined by identifying the peak subunits in the DLPFC area with the most negative connections to the sgACC area in the original study. For more details on this dataset, see Li et al. [53].

The fourth dataset ("CUD-TMS") comprises 27 cocaine use disorder (CUD) patients who underwent two daily sessions of rTMS treatment over the left DLPFC in an acute phase and two weekly sessions of rTMS treatment in a maintenance phase. The rTMS treatment was delivered at the left DLPFC using either the 5.5 cm anatomic criterion or the Beam F3 method. Depressive symptoms were a secondary treatment outcome in the original study. A subsample of 16 individuals, all with baseline HAMD scores above 7, was used for further calculation of individualized TMS targets. The TMS outcomes, neuroimaging data, participants' demographic info, and target coordinates for this dataset were openly shared (https://openneuro.org/datasets/ds003037/versions/1.0.0). For more details on this dataset, see Garza-Villarreal et al. [54].

Approach

The study's first objective was to delineate case-control differences in the sgACC-FC profile and explore its implication in identifying FC-guided individualized TMS targets. Accordingly, we conducted a generalized linear model (GLM) to compare voxel-wise sgACC-FC maps of MDD patients and HCs in the DIRECT dataset. We then demonstrated the association

between clinical improvement and group differences in TMS targeting sgACC-FCs by leveraging the TRD-TMS and SID-TMS datasets. Given that the peak sgACC anticorrelation of a normative connectome within the left DLPFC was usually selected as the FC-guided sgACC group target, we showed the impact of case-control differences on such group targets by separately identifying the peak sgACC anticorrelation in the mean sgACC-FC maps of the MDD group and HC group from the DIRECT dataset. Finally, we identified individualized optimal targets using the MDD big data-guided individualized TMS targeting algorithm guided by statistical maps (e.g., group difference map, mean sgACC-FC maps). We validated the clinical effectiveness of the individualized approach by computing the correlation between clinical outcomes and the distance between the actual TMS sites and the identified individualized targets in the SID-TMS and CUD-TMS datasets. All statistical tests conducted in the current study were two-sided.

Power calculations for primary hypotheses

The primary outcome of the current study is the case-control differences regarding the sgACC-FC profiles. Estimates of the effect size (Cohen's d = 0.186) of MDD patients' abnormalities in FCs are drawn directly from our prior research based on the DIRECT Phase I dataset [24]. Power calculation was performed using R version 4.3.1 [55] with pwr [56]. A sample of 455 patients will achieve 80% power with a 5% Type I error rate.

Image preprocessing

Acquisition parameters and scanners for all cohorts are provided in Table S2. All R-fMRI and structural MRI scans were preprocessed at each site using the same DPABISurf protocol, an R-fMRI data analysis toolbox evolved from DPABI/DPARSF [32,57,58] (For details, see SI). Given the controversy regarding global signal regression (GSR) and its essential role in identifying TMS targets [41], we performed preprocessing pipelines with and without GSR.

315 **FC maps of sgACC**

316 Although recent studies have attempted to identify personalized TMS targets using
317 surface-based algorithms [44], most previous studies have reported targets in volume-based
318 MNI space with sgACC ROIs defined as a sphere in volume-based space [36,59]. As a result, we
319 used the volume-based preprocessed imaging data from DPABISurf to better compare our
320 results with the existing literature.
321
322 We defined the sgACC as a 10 mm diameter sphere located on the average MNI coordinates
323 based on prior studies showing reduced glucose metabolism or blood flow after receiving an
324 antidepressant treatment (MNI coordinates: x = 6, y = 16, z = -10. For details, please refer to
325 Fox et al., 2012 [36]). The sgACC time series were determined for each individual by spatially
326 averaging the preprocessed R-fMRI time series across all voxels in the abovementioned
327 masks. We then calculated whole-brain FC maps in volume-based MNI space. FC was
328 calculated using Pearson's correlation and underwent Fisher's r-to-z transformation. All FC
329 maps were smoothed with a 6 mm full-width half maximum (FWHM) kernel size. We used
330 ComBat [60] to control potential site and scanner biases (For details, see SI).

331 **Group difference maps of sgACC-FC profiles**

332 We used a voxel-wise GLM to examine differences in the FC maps of sgACC between MDD
333 patients and HCs in DIRECT Phase II. Cohen's f^2 was calculated to characterize the effect sizes
334 of this group difference effect. The GLM model includes age, sex, education, and head
335 motion as covariates:

336 $$\boldsymbol{y} = \boldsymbol{\mu} + \boldsymbol{X\beta} + \boldsymbol{\epsilon} \quad (1)$$

337 where y denotes the FC value of a given voxel from a given participant; $\boldsymbol{\mu}$ stands for the
338 constant term; X represents the design matrix for the covariates of interest (diagnosis, age,
339 sex, education, and head motion); $\boldsymbol{\beta}$ is a vector of regression coefficients corresponding to X;
340 and $\boldsymbol{\epsilon}$ is a vector of residuals that follow $N(0, \boldsymbol{\sigma}^2)$. Multiple comparison correction was
341 conducted using false discovery rate (FDR) correction at $q < 0.05$.

To further interpret group difference maps, we extracted the mean FC values of seven networks using Schaefer's 400 parcellation atlas [61]. A GLM model identical to model (1) was constructed to characterize case-control differences for each network. Bonferroni multiple comparison correction was conducted ($p < 0.05/7$). We further explored the effect of the identified DLPFC clusters in several subgroups. Specifically, patients who were in their first episode and had never received any antidepressant medication treatment (first episode drug naïve, FEDN, N = 484) and patients who had undergone more than one episode (recurrent, N = 439) were selected and compared. Three contrasts, FEDN vs. HC, recurrent vs. HC, and FEDN vs. recurrent, were analyzed.

Relationship between group differences in TMS targets' sgACC FCs and clinical outcomes

To explore the relationship between group differences in TMS targets' sgACC FCs and clinical outcomes, we first extracted the mean *t*-values from the group difference map of 8 mm radius spheres centered at each targeting coordinate in the TRD-TMS dataset, then examined the Pearson correlations between these *t*-values and HAMD score reductions. We anticipated that greater group differences in sgACC-FC at the target location (i.e., higher *t* values) would be related to better TMS therapeutic effects (higher HAMD reductions). To test the robustness of our findings, we also used spheres with 2 mm, 4 mm, and 10 mm radiuses to extract the *t*-values of group differences.

Group targets based on mean sgACC-FC maps

The prior group-level DLPFC TMS target had been derived from a cohort of healthy young adults [38]; here, we separately averaged whole-brain sgACC-FC maps across all the DIRECT participants in the MDD and HC groups. We then searched for the peak sgACC anticorrelated voxel within the DLPFC area (i.e., Brodmann area (BA) 46) as the mean sgACC-FC guided TMS targets for the MDD and HC groups.

Identification of individualized TMS targets

The reliable statistical maps from the DIRECT big sample best reflect the probability of MDD-related abnormalities in sgACC-FC. Therefore, we can use these maps to guide the identification of individualized abnormalities by combining this big-data-based abnormality information with the individualized R-fMRI data from a given patient, obtaining reliable statistical maps from the DIRECT sample. We used the dual regression approach to identify individualized TMS targets guided by group-level statistical maps in the SID-TMS and CUD-TMS datasets. Dual regression is a common method in independent component analysis (ICA) for projecting group-level independent components (e.g., functional networks) onto the individual subject level (see Figure S4 for details). In the first step of the MDD big data-guided individualized TMS targeting algorithm, a group-level statistical spatial map (e.g., the sgACC-FC group difference map reflecting the probability of MDD-related abnormalities in sgACC-FC) was used as a spatial regressor in the GLM to identify the temporal dynamic of the group-level map (similar to spatial correlation with the abnormality spatial map). A time series associated with the spatial map of MDD-related FC abnormalities was generated. In the second step, the derived time series was used as a temporal regressor in the GLM to identify an individual-level spatial map (similar to the temporal correlation with the previous time series). This spatial map can be considered the best-individualized abnormality guided by big-data-based abnormality. Given our prior knowledge of DLPFC TMS treatment in MDD, we confined the big-data-based abnormality dual regression to the DLPFC area. That is, we use the group DLPFC abnormality probability map to find the individualized DLPFC target in a given MDD patient. The final coordinates for the individualized TMS targets are defined as the centroids of the largest clusters within this DLPFC region on the individual-level spatial maps. Additionally, we calculated the individualized target coordinates using the seed map approach, following the methods described by Fox et al. [41] and Cash et al. [44]. In the seed-map approach, a seed time series is extracted by computing a weighted average time series of all voxels within the seed map (e.g., a group average map of sgACC-FC, but excluding the DLPFC area). Subsequently, Pearson's correlation coefficients are computed between this extracted

time series and all other DLPFC voxels. The final TMS target is the most negatively functionally connected cluster in the DLPFC area. Of note, in the seed map approach, the goal of the first step is to find the most sgACC-like time series, which is not confined to the noisy sgACC area. Following this rationale, the DLFPC time series should not be included to avoid biasing the estimation of the sgACC-like time series. Thus, the DLPFC area was excluded. Thus, the exclusion and inclusion of DLPFC differs between the seed map approach and the DR approach due to the different underlying rationales. Details of the individualized TMS target localization algorithms are provided in the supplementary materials.

Clinical efficacy of the group-level and individualized TMS targets

We leveraged the SID-TMS and CUD-TMS datasets to evaluate the clinical significance of individualized TMS targets. We identified the proposed individualized TMS targets from the MDD big data-guided individualized TMS targeting algorithm and calculated the targeting offset (i.e., Euclidean distance between the individualized optimal TMS targets and the actual stimulation coordinates) for each patient. Subsequently, we calculated the Pearson correlations between clinical improvement (i.e., HAMD reductions) and targeting offset. We anticipated a negative correlation between clinical outcomes and target offset (i.e., the closer the actual stimulation target was to the individualized target from the MDD big data-guided individualized TMS targeting algorithm, the higher the clinical improvement). Age, sex, and head motion were included as covariates in the regression models when calculating correlations between targeting offsets and clinical improvement.

Results

Group difference maps of sgACC-FC

In the large-scale DIRECT Phase II dataset, we found significant MDD-related hyperconnectivity with the sgACC in bilateral DLPFC, temporal parietal junction, and occipital

lobe, as well as hypoconnectivity in the bilateral temporal lobe, left inferior frontal gyrus, and left postcentral gyrus when preprocessing included GSR (Figure 2A). When GSR was not included in preprocessing, MDD-related sgACC FC alterations showed predominantly hypoconnectivity. Such abnormally decreased FCs were found across the central gyrus, occipital lobe, insular cortex, temporal lobe, and a small portion of the frontal lobe. Without GSR, MDD-related hyperconnectivity was limited to subcortical regions (Figure S1A). Given that significant case-control differences in the DLPFC area were revealed only when GSR was implemented, subsequent analyses were based on results with GSR. The uncorrected group difference maps calculated in the volume space showed remarkable similarity with those in the surface space (Figure S2). Network-wise FC analyses showed that MDD patients' FC between sgACC and the limbic network (LN) was significantly reduced compared to HC ($t(2880) = -4.122$, $p_{corrected} < 0.001$, Cohen's $d = 0.171$). The FC between sgACC and the frontoparietal network (FPN) was enhanced and approached significance ($t(2880) = 2.419$, $p_{corrected} = 0.055$, Cohen's $d = 0.090$, Figure 2B). Without GSR, MDD patients showed decreased FC between sgACC and all brain networks (all $p_{corrected} < 0.05$) except for the FPN (Figure S1B). We identified two contiguous clusters of voxels that showed significant group differences in the left DLPFC. Group difference cluster 1 (MNI coordinates: x = -44, y = 38, z = 32; $t(2880) = 3.277$, $p < 0.001$, Cohen's $d = 0.141$) was ventral to group difference cluster 2 (MNI coordinates: x = -34, y = 36, z = 40; $t(2880) = 3.670$, $p < 0.001$, Cohen's $d = 0.126$) (Figure 2C). In subgroup analyses, when GSR was performed, FEDN patients showed enhanced FCs in both clusters (cluster 1: $t(1790) = 2.282$, $p = 0.023$, Cohen's $d = 0.124$; cluster 2: $t(1790) = 2.273$, $p = 0.023$, Cohen's $d = 0.123$). There was a significant enhancement in the DLPFC cluster 2 between the recurrent MDD patients and HCs ($t(1745) = 2.765$, $p = 0.006$, Cohen's $d = 0.159$) while cluster 1 approached significance ($t(1745) = 1.864$, $p = 0.063$, Cohen's $d = 0.107$). No significant difference was revealed between the FEDN and recurrent patients (see Figure 3).

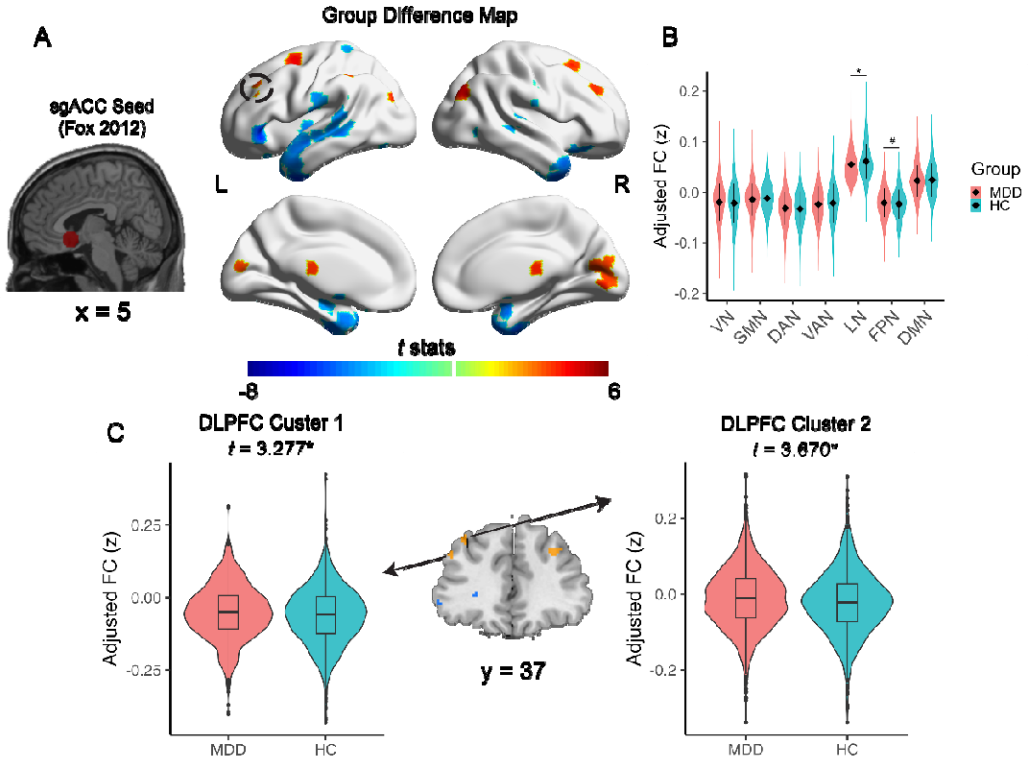

Figure 2. Group differences of subgenual anterior cingulate cortex (sgACC) functional connectivity (FC) profiles are related to TMS treatment efficacy, demonstrating clinical significance. (A) Two-sample *t*-test maps of MDD-related sgACC FC abnormalities with global signal regression (GSR) implemented. (B) Group differences of FCs between sgACC and visual network (VN), somatomotor network (SMN), dorsal attention network (DAN), ventral attention network (VAN), limbic network (LN), frontoparietal network (FPN), and default mode network (DMN). (C) Two clusters showed significant case-control differences in sgACC-FC. Abbreviations: DLPFC, dorsal lateral prefrontal cortex; L, left hemisphere; R, right hemisphere. *: significant after Bonferroni correction; #: approaching significance.

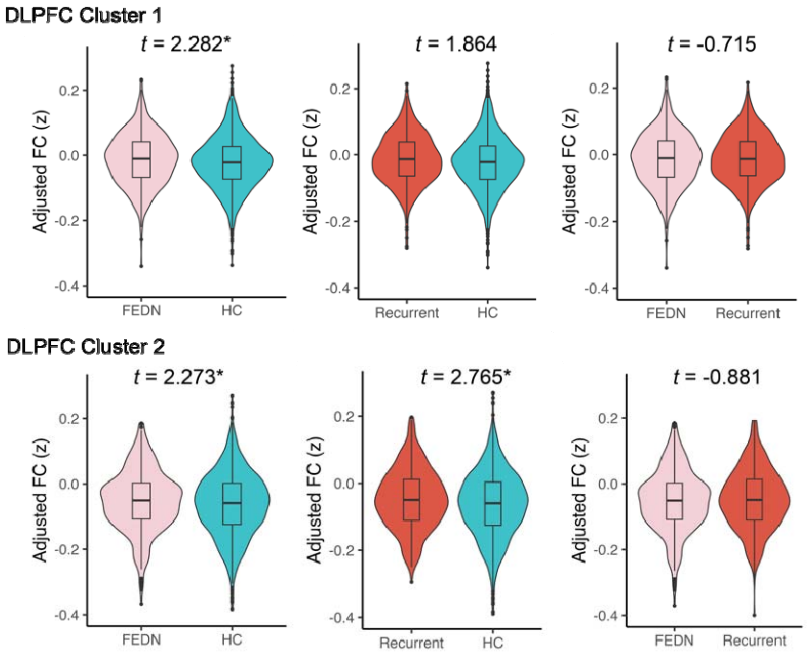

458

459 Figure 3. Subgroup differences regarding two clusters found in DLPFC. Abbreviations: FEDN, first

460 episode drug naïve; HC, healthy control.

461

462 **sgACC anticorrelation peaks in MDD and HCs**

463 Our results highlighted the case-control differences in sgACC-FC profiles. Since the prior

464 sgACC group target (MNI coordinates: x = −42, y = 44, z = 30) had been based on a cohort of

465 young, healthy adults [38], we sought to examine potential differences in anticorrelation peaks

466 extracted from the mean sgACC FC maps of MDD and HC groups (Figure 4B-C) in the DIRECT

467 dataset. We found that the anticorrelation peak of MDD patients (MNI coordinates: x = -40, y

468 = 50, z = 22) differed from that of HCs (MNI coordinates: x = -42, y = 38, z = 32), probably due

469 to abnormal FCs within the left DLPFC in MDD patients. The anticorrelation peak extracted

470 from the DIRECT HCs was closer to the previously reported locus [38] (Figure 4).

471

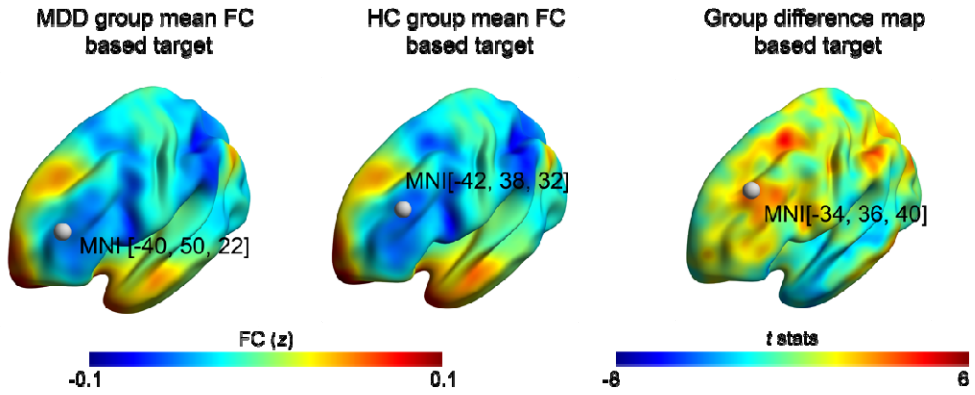

Figure 4. The peak of the sgACC anticorrelation in MDD patients differed from that in HCs.

sgACC-FC group differences correlate with TMS treatment outcomes

Using the TRD-TMS dataset, we examined the relationship between group differences (*t*-values) and clinical outcomes (HAMD reductions) to test the clinical relevance of the group difference maps. Group differences were positively correlated with HAMD score reductions ($r(23) = 0.448$, $p = 0.025$, Figure 5A), suggesting that group-level difference maps may be useful for enhancing the outcomes of TMS for treating MDD by improving target localization. Significant associations were also observed using different radius settings (Figure S11). The same trend was observed in the SID-TMS dataset, albeit it failed to achieve significance ($r(26) = 0.304$, $p = 0.108$, Figure 5).

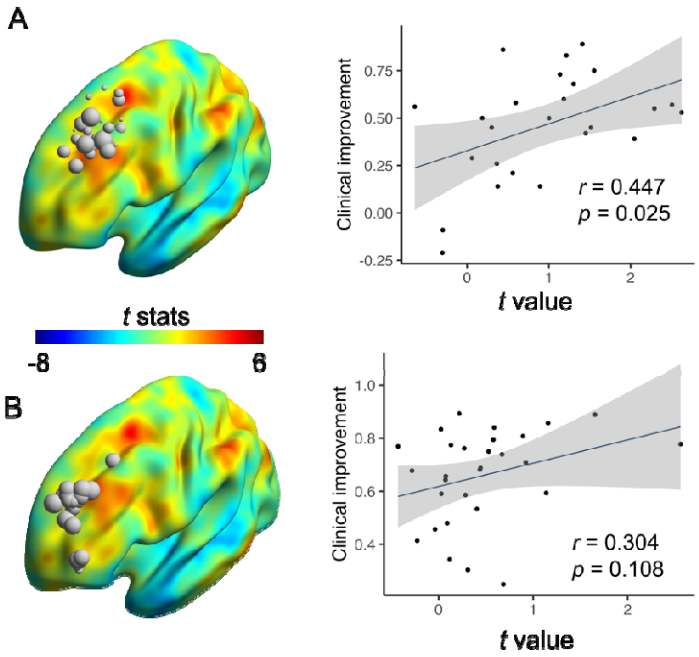

Figure 5. The group difference regarding sgACC-FC to the TMS targets was correlated with clinical efficacy. (A) The TMS targets were extracted from the TRD-TMS dataset [38]. The sizes of the spheres indicate the magnitudes in Hamilton Depression Rating Scale (HAMD) reductions, with the group difference map rendered on the surface. The scatter plot depicted that the magnitudes of the group differences in the FC between TMS targets and sgACC were positively related to clinical improvements in the TRD dataset. (B) Findings were replicated in the SID-TMS dataset [53]. Abbreviations: FC, functional connectivity; TMS, transcranial magnetic stimulation.

Individualized targets suggest higher clinical efficacy than group targets

We utilized the MDD big data-guided individualized TMS targeting algorithm to calculate individualized optimal targets for each SID-TMS and CUD-TMS dataset participant. Clinical relevance of the targets was determined by the correlation between target offset and clinical improvement. The individualized target locations derived from the sgACC-FC group difference map are illustrated in Figure 6. The individualized targets (SID-TMS: $r(26) = -0.562$, $p = 0.002$; CUD-TMS: $r(14) = -0.511$, $p = 0.037$) outperformed their corresponding group-level targets (SID-TMS: $r(26) = -0.349$, $p = 0.044$; CUD-TMS: $r(14) = -0.167$, $p = 0.293$) in both

datasets (Figure 6). The DR-based individualized targets derived from the MDD or HC group-average sgACC-FC maps also outperformed their corresponding group-level targets and seed map-based targets (Figure S6-8). Among all the individualized targets, the DR-based targets guided by the group difference map achieved the highest clinical efficacy.

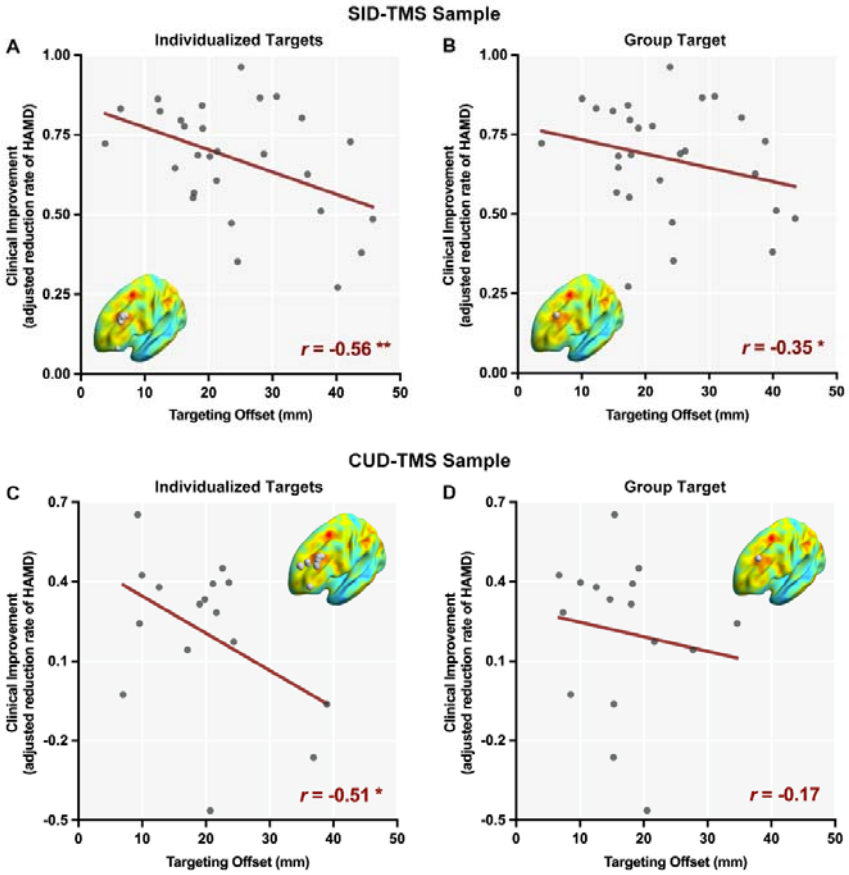

Figure 6. Individualized targets derived from the group difference map exhibited greater clinical efficacy than the corresponding group targets. Clinical efficacy was characterized by computing the correlations between the offset distances of TMS targets and the clinical improvements observed in the CUD-TMS dataset. The TMS targeting offset distance was defined as the Euclidean distance between the actual rTMS stimulation coordinates and the individualized or group targets. Clinical improvement was defined as the HAMD reduction during rTMS treatment, adjusted for age, sex, and head motion. The locations of the targets are displayed on the cortex. The sizes of the spheres indicate the magnitudes of Hamilton Depression Rating Scale (HAMD) reductions. (A-B) Clinical efficacy of the

individualized and group targets in the SID-TMS sample. (C-D) Clinical efficacy of the individualized and group targets in the CUD-TMS sample. *$p < 0.05$. ** $p < 0.01$.

Discussion

In the present study, we leveraged a large multi-site fMRI sample (1660 MDD patients and 1341 HCs) and three independent TMS datasets to delineate abnormalities in sgACC FC in MDD and explore their potential impact on the localization of TMS targets. Specifically, with GSR implemented, we found enhanced FCs between sgACC and left DLPFC, bilateral supplementary motor areas and inferior parietal lobes, thalamus, and visual areas, and decreased FCs between sgACC and left anterior insula, left superior temporal lobe, and bilateral temporal poles in MDD patients. Patients with MDD exhibited significantly reduced FC between the sgACC and the DMN, while FC between the sgACC and the FPN was only marginally increased. Crucially, we showed that the clinical outcomes of TMS treatments were related to the magnitude of the case-control differences in the FCs between sgACC and TMS targets. Furthermore, such group difference profiles altered the position of the sgACC anti-correlation peak in the left DLPFC. Additionally, the MDD big data-guided individualized TMS targeting algorithm to identify individualized TMS targets showed better clinical efficacy than TMS targets based on group sgACC-FC profiles.

MDD-related FC abnormalities of sgACC

Our results add to a growing literature documenting functional network abnormalities involving the sgACC in MDD [9,11-13,17,19,62-64]. Nevertheless, notable discrepancies in the type of abnormality (enhanced/reduced) and specific brain regions showing altered sgACC FCs have been reported. Considering the small effect sizes (Cohen's $f^2 < 0.01$) of MDD-related sgACC-FC abnormalities, the limited sample sizes in previous studies entail a high risk of false positive findings [21,65,66]. Another potential source of heterogeneity in previous findings may be whether or not they applied GSR (See supplementary materials for detailed discussion).

With an unprecedented sample size, our results provide among the most robust evidence to date. Specifically, MDD patients showed enhanced sgACC-thalamus FC and decreased sgACC-limbic network FC regardless of whether GSR was implemented. These results are consistent with previous studies in adolescents [19] and adults [59] with MDD. Previous studies have reported abnormal FCs between sgACC and limbic areas and some subcortical regions, such as the amygdala [9,20] and parahippocampus regions [13]. Together, the present results are consistent with a model highlighting sgACC as a critical hub in an "extended medial network," which also encompasses limbic, thalamic, and striatal regions and plays a key role in the pathophysiology of MDD [67,68]. This "extended medial network" overlaps substantially with the DMN. Indeed, decreased FCs between sgACC and DMN regions, such as the medial prefrontal cortex, precuneus, temporal gyrus, and parahippocampus regions, were revealed in MDD relative to HCs when GSR was not implemented. Such abnormalities have been previously reported [10,12,15,34], which led to the hypothesis that abnormally enhanced FC between sgACC and DMN are the network underpinnings of rumination [69]. However, contrary to the aforementioned hypothesis, we found reduced, instead of enhanced FC between sgACC and DMN. Similarly, in the first phase of DIRECT, we demonstrated that MDD was characterized by reduced FC within DMN [23,24]. We note that the first and second phases of the DIRECT data are solely comprised of Chinese samples, while most studies that have reported enhanced sgACC-DMN FCs have been in Caucasian samples. Different prevalence rates [70,71], heterogeneous symptoms [72], and different risk alleles [73] have been reported in Caucasian and Eastern Asian groups. Accordingly, we cannot exclude racial differences contributing to this discrepancy. It is worth noting that we found enhanced FCs between the visual region and sgACC in MDD patients relative to HCs when GSR was implemented, while significantly reduced sgACC-visual region FCs were revealed when GSR was not performed. Most of DIRECT II sites' R-fMRI data were collected with participants' eyes closed (22 out of 23 sites). Prior research had shown that participants are more likely to fall asleep when their eyes are closed during data acquisition, and drowsiness may alter FC patterns in visual regions [74]. Thus, it is possible that abnormalities in visual region FCs may be due to MDD patients' lower levels of wakefulness.

Clinical relevance of abnormal sgACC-DLPFC anticorrelation in MDD

Once the group difference maps of sgACC FC profiles were delineated, we further explored the impact of such an abnormality, especially in DLPFC, on identifying TMS targets. Most clinical trials have focused on applying TMS to the left DLPFC based on the hypothesis that high-frequency rTMS will enhance hypoactivity during depressive episodes [8,75]. The DLPFC is anatomically extensive [76]. However, which DLPFC sub-field is the best target for TMS remains unclear. The current FDA-approved protocol (i.e., the "5 cm" method) leads to large interindividual variation in stimulation sites, which may contribute to the heterogeneity in the effect sizes of antidepressant responses in prior trials [77,78].

Previous targeting approaches leveraging anatomical landmarks has not consistently outperformed the "5 cm" method or the F3 Beam method [79,80]. Considering the unsatisfactory effect of TMS target localization based on brain anatomical parcellation, group-level normative sgACC anticorrelation peaks based on healthy population datasets have been frequently used as TMS targets in recent years [36,38,41]. However, in the present study, we found that the locations of such anticorrelated peaks differ substantially between MDD and HC samples when measured in a large clinical cohort. Therefore, it might be problematic to identify TMS targets based solely on sgACC-FC profiles in healthy or depressed individuals. Intriguingly, we found that the magnitudes of case-control differences in TMS targets' FCs to sgACC were positively related to the clinical improvements after receiving rTMS to the left DLPFC. Such correlation implies that the case-control differences in the FC between sgACC and the left DLPFC might bear important information that could be leveraged to guide the identification of reliable, individualized TMS targets.

The MDD big data-guided individualized TMS targeting algorithm may improve the clinical efficacy of TMS targets

In the current study, we developed an MDD big data-guided individualized TMS targeting algorithm to individualize the TMS targets derived from group-level statistical maps. The

proposed approach takes advantage of the high signal-to-noise ratio and reliability of large sample statistical maps while integrating individual spontaneous brain activity of individuals with MDD. Most existing individualized TMS target localization algorithms are based on calculating sgACC FCs using densely sampled MRI images from single subjects [81]. However, individual MRI images tend to be noisy and unreliable [82,83], especially in the sgACC region. Air in the sinuses often introduces susceptibility artifacts due to the different magnetic properties of air and brain tissue. Signal loss and geometric distortion are common in areas close to air-filled sinuses, such as the inferior frontal cortex, including the sgACC [84]. The seed map approach has been proposed to alleviate such difficulties due to the subpar image quality of the sgACC region [41,44]. In the seed map approach, all voxels within the seed map (except for the DLPFC region) were used to extract the seed time series to improve its signal-to-noise ratio. However, considering that the weight (e.g., FC value) of the sgACC area is usually extremely high in the seed map, the derived seed time series remains somewhat similar to the noisy sgACC time series and doesn't achieve the best TMS localization. A cutting-edge MDD TMS therapy combining FC-guided target localization, high dose, and intermittent theta-burst stimulation (iTBS) was reported to be highly effective in a randomized, double-blinded, sham-controlled clinical trial [45,46]. However, the targeting algorithm relied on hierarchical agglomerative clustering in the sgACC area which has a low signal-to-noise ratio. Nevertheless, the final target was still determined according to individual-level sgACC-DLPFC FCs. For the proposed MDD big data-guided individualized TMS targeting algorithm, we view the reliable statistical maps from the DIRECT big sample as the best reflection of the probability of MDD-related abnormalities in sgACC-FC. Therefore, we used these maps to guide the identification of individualized abnormalities by combining this big-data-based abnormality information with the individualized R-fMRI data from a given patient. Given the a priori knowledge of DLPFC TMS treatment in MDD, we confined the big-data-based abnormality dual regression only within the DLPFC area, which is less affected by susceptibility artifacts. In this way, the superior signal quality of DLPFC and the effective and reliable properties of the dual regression algorithm enhance the accuracy of target localization.

627

628 Encouragingly, the DR-based individualization targets enhanced the clinical significance of
629 corresponding group-level targets, regardless of the template used. This result supports the
630 generalizability and extensibility of the algorithm, offering the potential for TMS targeting
631 based on other circuits and biomarkers. Considering most existing TMS research still relies on
632 the traditional 5 cm or Beam F3 methods for targeting, one approach based on our data to
633 improve targeting would be simply shifting the target to a more anterior and lateral position.
634 However, such a simple shift was not supported by the present study. Instead, 25% of targets
635 individualized using the group difference map were more medial than the original targets,
636 and 50% of targets individualized by the group difference map were more posterior than the
637 original targets. Therefore, the MDD big data-guided individualized TMS targeting algorithm
638 does not simply set a more anterior and lateral coordinate in the BA46 area as the
639 individualized optimization target for subjects. Among the group-level templates used in the
640 MDD big data-guided individualized TMS targeting algorithm, the sgACC-FC group difference
641 map performed the best, instead of the commonly used average sgACC based on healthy
642 individuals. This may reflect the abnormal posterior shift of the MDD sgACC anticorrelation
643 peak we found, and it emphasizes the immense clinical value of examining spontaneous
644 brain activity differences between MDD and HC in a large sample. Previous studies either
645 included only a small quantity of MDD functional MRI data [46,47,85] or developed targeting
646 algorithms based on large-scale HC samples [49]. In this study, we utilized an unprecedented
647 amount of functional MRI data from MDD and HC, obtained a reliable group-level difference
648 map of sgACC-FC, and successfully validated its potential in treating MDD with TMS.
649

650 **Limitations**

651 Several limitations need to be considered. First, we noted that the inconsistency between
652 our results and the broader literature could partly be due to racial differences of the samples
653 (i.e., Eastern Asian vs. Caucasian). Efforts that intend to pool existing neuroimaging data
654 worldwide, such as the Enhancing NeuroImaging Genetics through Meta-Analysis (ENIGMA)

Major Depressive Disorder (MDD) consortium [25], have accumulated large-scale data primarily from Western countries and published several high-impact studies delineating MDD-related anatomical abnormalities [86,87]. Planned collaborations between the DIRECT and the ENIGMA-MDD consortiums are ongoing to help address potential cultural, genetic, and environmental mechanisms in more diverse groups of MDD patients. Second, we performed volume-based preprocessing to facilitate comparison with the previous literature. Surface-based preprocessing strategies have provided more accurate and detailed representations of cortical and subcortical structures [88]. Recent research has begun to explore surface-based rTMS target identification algorithms and has shown promising clinical relevance [39,40,89]. Future research should consider using surface-based case-control difference maps to further refine ways to identify TMS targets. Given the established involvement of the left DLPFC in existing TMS treatment protocols, the present study restricted investigation to within this area.

We noted that other brain regions (e.g., angular gyrus and supplementary motor area) showed significant case-control differences worth further research and may serve as potential targets for neuromodulation [90,91 92]. The MDD big data-guided individualized TMS targeting algorithm can be readily transferred to other neural circuits or other brain imaging-derived feature maps (e.g., ICA, functional gradient, normative modeling). The clinical efficacy of these alternative targets is worthy of future investigations. Identifying a reliable personalized TMS target solely based on an individual's R-fMRI data (around 8 mins of fMRI scan in clinical practice) is challenging. Due to the poor replicability of FC [93], existing individual-level network parcellation algorithms need a large quantity of fMRI images (usually more than one hour of scanning time) [94]. The present study utilized three independent TMS samples to validate the efficacy of the individualized algorithm. Nevertheless, the two TMS datasets used to validate the individualized TMS targets are limited in sample size [37,95]. Publicly available TMS brain imaging datasets could be used for independent validation of target localization algorithms to reduce the false positive rate; however, access to such datasets remains challenging. In addition, prospective, double-blind

clinical trials are warranted to compare the treatment outcome across different rTMS targeting algorithms (e.g., traditional anatomical landmark-based targeting, group-level sgACC-FC targeting, and MDD big data-guided individualized TMS targeting algorithm). Therefore, we call upon researchers involved in this field to publicly share data on TMS targets, clinical efficacy, and brain imaging, and we will also openly share data from our related prospective studies [96]. The large sample size of the DIRECT consortium aggregated dataset allows for intriguing analyses, such as bio-subgroups of MDD patients. Indeed, some previous DIRECT studies have shown that MDD patients can be subgrouped [30,97]. Future studies may further determine whether bio-types could be achieved using sgACC [91]. Most of the DIRECT II R-fMRI data were acquired when participants were instructed to close their eyes, which has been shown to be associated with an increased likelihood of sleep during scanning [74]. Instructing participants to keep their eyes open and look at fixation can help prevent participants from falling asleep and is easy to apply. Since large multi-site R-fMRI data aggregation endeavors such as DIRECT are prone to be biased by non-neurophysical factors such as head motion, sleepiness, etc. [98], it is important to prospectively apply well-designed standard operation procedures in future large-scale multi-site scientific projects.

Conclusion

In summary, we leveraged a large sample of MDD patients to fully delineate group differences in sgACC-FC maps between MDD patients and HCs. We next demonstrated the impact of such case-control differences on group TMS targets based on sgACC-FC profiles by showing that the magnitudes of case-control differences in the FC between sgACC and TMS targets were positively associated with clinical outcomes and the peak sgACC anticorrelation locations were different in MDD patients as compared to HCs. Moreover, we developed an MDD big data-guided individualized TMS targeting algorithm to identify individualized TMS targets and demonstrated that this approach may improve clinical efficacy compared to group targets based on sgACC-FC profiles.

Contributors

C-GY, Y-FZ, X-NZ, XC, and BL conceived and designed the study. C-GY, Y-FZ, J-PZ, and X-NZ coordinated the collaboration. JQ, LK, T-MS, TL, K-RZ, Z-NL, L-PC, JY, X-PW, Y-GY, C-YW, C-MX, G-RX, Y-SL, Y-QY, XW, YW, X-FX, Y-QC, Q-YG, W-BG, J-PZ, YH, H-NW, B-JL, WZ, and J-PL supervised data collection. X-RW, QH, Y-KW, HY, A-XZ, Y-CL, J-SC, P-FS, X-YL, FL, C-CH, X-LC, F-NJ, J-JZ, X-LJ, G-MC, Z-SC, T-LC, X-XS, TC, B-JL, M-LY, Z-PX and BL organized the data. XC and C-GY analyzed and interpreted the data. BL and C-GY designed the dual regression-based TMS targeting algorithm. H-NW and B-JL collected the SID-TMS dataset. XC, BL, and C-GY drafted the manuscript. All authors revised the manuscript for important intellectual content and approved the final submitted version. XC, BL, and C-GY accessed and verified the data. XC, BL, and C-GY had full access to all the data in the study. C-GY had final responsibility for the decision to submit for publication. All authors were responsible for the final decision to submit for publication and have seen and approved the manuscript.

Conflict of interest

DMB receives research support from the Canadian Institutes of Health Research (CIHR), National Institutes of Health – US (NIH), Brain Canada Foundation, and the Temerty Family through the CAMH Foundation and the Campbell Family Research Institute. He received research support and in-kind equipment support for an investigator-initiated study from Brainsway Ltd., and he was the site principal investigator for three sponsor-initiated studies for Brainsway Ltd. He received in-kind equipment support from Magventure for investigator-initiated studies. He received medication supplies for an investigator-initiated trial from Indivior. He has participated in an advisory board for Janssen. He has participated in an advisory board for Welcony Inc. No other conflicts of interest.

Inclusion and Ethics

Local researchers were included throughout the research process. Research protocols have been approved by local ethics review committees. No potential risk was involved in the current research, and all local researchers have discussed and approved the research protocol. All participants provided written informed consent, and local institutional review boards approved each study from all included cohorts. The analysis plan of the current study has been reviewed and approved by the Institutional Review Board of the Institute of Psychology, Chinese Academy of Sciences (No. H21102).

Data Sharing

According to the success of the data sharing model of DIRECT Phase I data (REST-meta-MDD, http://rfmri.org/REST-meta-MDD), DIRECT Phase II data will also have 2 sharing stages. 1) Stage 1: coordinated sharing upon the publication of this announcing manuscript. To reduce conflict among the researchers, the consortium will review and coordinate the proposals submitted by interested researchers. The interested researchers first send a letter of intent to rfmrilab@gmail.com. Then, the consortium will send all the approved proposals to the applicant. The applicant should submit a new innovative proposal while avoiding conflict with approved proposals. The consortium would review and approve this proposal if there is no conflict. Once approved, this proposal would enter the pool of approved proposals and prevent future conflict. 2) Stage 2: unrestricted sharing after January 1, 2026. The researchers can perform any analyses of interest while not violating ethics. All codes have been made openly available (https://github.com/Chaogan-Yan/PaperScripts/tree/master/Chen_2023).

Acknowledgments

This work was funded by the Sci-Tech Innovation 2030 - Major Project of Brain Science and

764 Brain-inspired Intelligence Technology (No. 2021ZD0200600), the National Key R&D Program
765 of China (No. 2017YFC1309902), the National Natural Science Foundation of China (No.
766 82122035, No. 81671774 and No. 81630031), the Key Research Program of the Chinese
767 Academy of Sciences (No. ZDBS-SSW-JSC006), Beijing Nova Program of Science and
768 Technology (No. Z191100001119104 and 20230484465), Beijing Natural Science Foundation
769 (J230040), the Scientific Foundation of Institute of Psychology, Chinese Academy of Sciences
770 (No. E2CX4425YZ and No. Y9CX422005), the China Postdoctoral Science Foundation (No.
771 2019M660847), the China National Postdoctoral Program for Innovative Talents (No.
772 BX20200360), the Special Research Assistant Program of the Chinese Academy of Sciences
773 (No. E2CX0624) and the Key R&D Program of Sichuan Province (No. 2023YFS0076). The
774 support provided by the China Scholarship Council (CSC, No. 202104910248) during a visit of
775 Xiao Chen to the Centre for Addiction and Mental Health is acknowledged. In addition, we
776 would like to acknowledge the valuable insights provided by Prof. B.T. Thomas Yeo, whose
777 comments helped to shape our understanding of the data and refine our analysis.
778

779 **References**

780 1. Malhi GS, Mann JJ. Depression. *Lancet (London, England)* 2018; **392**(10161): 2299-312.
781 2. Drevets WC, Price JL, Furey ML. Brain structural and functional abnormalities in mood
782 disorders: implications for neurocircuitry models of depression. *Brain structure & function*
783 2008; **213**(1-2): 93-118.
784 3. Disner SG, Beevers CG, Haigh EAP, Beck AT. Neural mechanisms of the cognitive model of
785 depression. *Nat Rev Neurosci* 2011; **12**(8): 467-77.
786 4. Mayberg HS. Modulating dysfunctional limbic-cortical circuits in depression: towards
787 development of brain-based algorithms for diagnosis and optimised treatment. *British*
788 *medical bulletin* 2003; **65**: 193-207.
789 5. Mayberg HS, Lozano AM, Voon V, et al. Deep brain stimulation for treatment-resistant
790 depression. *Neuron* 2005; **45**(5): 651-60.
791 6. Cash RFH, Zalesky A. Personalized and Circuit-Based Transcranial Magnetic Stimulation:
792 Evidence, Controversies, and Opportunities. *Biol Psychiatry* 2024; **95**(6): 510-22.
793 7. Cash RFH, Weigand A, Zalesky A, et al. Using Brain Imaging to Improve Spatial Targeting
794 of Transcranial Magnetic Stimulation for Depression. *Biol Psychiatry* 2020.
795 8. Fitzgerald PB. Targeting repetitive transcranial magnetic stimulation in depression: do
796 we really know what we are stimulating and how best to do it? *Brain Stimul* 2021; **14**(3):

730-6.
9. Connolly CG, Wu J, Ho TC, et al. Resting-State Functional Connectivity of Subgenual Anterior Cingulate Cortex in Depressed Adolescents. *Biological Psychiatry* 2013; **74**(12): 898-907.
10. Greicius MD, Flores BH, Menon V, et al. Resting-state functional connectivity in major depression: abnormally increased contributions from subgenual cingulate cortex and thalamus. *Biol Psychiatry* 2007; **62**(5): 429-37.
11. Wu H, Sun H, Xu J, et al. Changed Hub and Corresponding Functional Connectivity of Subgenual Anterior Cingulate Cortex in Major Depressive Disorder. *Front Neuroanat* 2016; **10**: 120.
12. Davey CG, Harrison BJ, Yucel M, Allen NB. Regionally specific alterations in functional connectivity of the anterior cingulate cortex in major depressive disorder. *Psychol Med* 2012; **42**(10): 2071-81.
13. Cheng B, Meng Y, Zuo Y, et al. Functional connectivity patterns of the subgenual anterior cingulate cortex in first-episode refractory major depressive disorder. *Brain imaging and behavior* 2021; **15**(5): 2397-405.
14. Sheline YI, Price JL, Yan Z, Mintun MA. Resting-state functional MRI in depression unmasks increased connectivity between networks via the dorsal nexus. *Proc Natl Acad Sci U S A* 2010; **107**(24): 11020-5.
15. Berman MG, Peltier S, Nee DE, Kross E, Deldin PJ, Jonides J. Depression, rumination and the default network. *Social cognitive and affective neuroscience* 2011; **6**(5): 548-55.
16. Wu X, Lin P, Yang J, Song H, Yang R, Yang J. Dysfunction of the cingulo-opercular network in first-episode medication-naive patients with major depressive disorder. *J Affect Disord* 2016; **200**: 275-83.
17. Sudheimer K, Keller J, Gomez R, et al. Decreased hypothalamic functional connectivity with subgenual cortex in psychotic major depression. *Neuropsychopharmacology* 2015; **40**(4): 849-60.
18. Davey CG, Yücel M, Allen NB, Harrison BJ. Task-related deactivation and functional connectivity of the subgenual cingulate cortex in major depressive disorder. *Frontiers in psychiatry* 2012; **3**: 14.
19. Gaffrey MS, Luby JL, Repovš G, et al. Subgenual cingulate connectivity in children with a history of preschool-depression. *Neuroreport* 2010; **21**(18): 1182-8.
20. Ho TC, Yang G, Wu J, et al. Functional connectivity of negative emotional processing in adolescent depression. *J Affect Disord* 2014; **155**: 65-74.
21. Button KS, Ioannidis JPA, Mokrysz C, et al. Power failure: why small sample size undermines the reliability of neuroscience. *Nat Rev Neurosci* 2013; **14**(5): 365-76.
22. Algermissen J, Mehler DMA. May the power be with you: are there highly powered studies in neuroscience, and how can we get more of them? *J Neurophysiol* 2018; **119**(6): 2114-7.
23. Chen X, Lu B, Li H-X, et al. The DIRECT consortium and the REST-meta-MDD project: towards neuroimaging biomarkers of major depressive disorder. *Psychoradiology* 2022; **2**(1): 32-42.
24. Yan CG, Chen X, Li L, et al. Reduced default mode network functional connectivity in

patients with recurrent major depressive disorder. *Proc Natl Acad Sci U S A* 2019.
25. Schmaal L, Pozzi E, T CH, et al. ENIGMA MDD: seven years of global neuroimaging studies of major depression through worldwide data sharing. *Transl Psychiatry* 2020; **10**(1): 172.
26. Yang H, Chen X, Chen ZB, et al. Disrupted intrinsic functional brain topology in patients with major depressive disorder. *Mol Psychiatry* 2021.
27. Long Y, Cao H, Yan C, et al. Altered resting-state dynamic functional brain networks in major depressive disorder: Findings from the REST-meta-MDD consortium. *Neuroimage Clin* 2020; **26**: 102163.
28. Ding YD, Yang R, Yan CG, et al. Disrupted hemispheric connectivity specialization in patients with major depressive disorder: Evidence from the REST-meta-MDD Project. *J Affect Disord* 2021; **284**: 217-28.
29. Deng K, Yue JH, Xu J, et al. Impaired robust interhemispheric function integration of depressive brain from REST-meta-MDD database in China. *Bipolar disorders* 2021.
30. Liang S, Deng W, Li X, et al. Biotypes of major depressive disorder: Neuroimaging evidence from resting-state default mode network patterns. *Neuroimage Clin* 2020; **28**: 102514.
31. Liu PH, Li Y, Zhang AX, et al. Brain structural alterations in MDD patients with gastrointestinal symptoms: Evidence from the REST-meta-MDD project. *Progress in neuro-psychopharmacology & biological psychiatry* 2021; **111**: 110386.
32. Yan C-G, Wang X-D, Lu B. DPABISurf: data processing & analysis for brain imaging on surface. *Science Bulletin* 2021.
33. Ge R, Downar J, Blumberger DM, Daskalakis ZJ, Vila-Rodriguez F. Functional connectivity of the anterior cingulate cortex predicts treatment outcome for rTMS in treatment-resistant depression at 3-month follow-up. *Brain Stimul* 2020; **13**(1): 206-14.
34. Cash RFH, Cocchi L, Anderson R, et al. A multivariate neuroimaging biomarker of individual outcome to transcranial magnetic stimulation in depression. *Hum Brain Mapp* 2019; **40**(16): 4618-29.
35. Philip NS, Barredo J, van 't Wout-Frank M, Tyrka AR, Price LH, Carpenter LL. Network Mechanisms of Clinical Response to Transcranial Magnetic Stimulation in Posttraumatic Stress Disorder and Major Depressive Disorder. *Biol Psychiatry* 2018; **83**(3): 263-72.
36. Fox MD, Buckner RL, White MP, Greicius MD, Pascual-Leone A. Efficacy of transcranial magnetic stimulation targets for depression is related to intrinsic functional connectivity with the subgenual cingulate. *Biol Psychiatry* 2012; **72**(7): 595-603.
37. Elbau IG, Lynch CJ, Downar J, et al. Functional Connectivity Mapping for rTMS Target Selection in Depression. *Am J Psychiatry* 2023; **180**(3): 230-40.
38. Weigand A, Horn A, Caballero R, et al. Prospective Validation That Subgenual Connectivity Predicts Antidepressant Efficacy of Transcranial Magnetic Stimulation Sites. *Biol Psychiatry* 2018; **84**(1): 28-37.
39. Cash RFH, Cocchi L, Lv J, Fitzgerald PB, Zalesky A. Functional Magnetic Resonance Imaging-Guided Personalization of Transcranial Magnetic Stimulation Treatment for Depression. *JAMA psychiatry* 2021; **78**(3): 337-9.
40. Siddiqi SH, Weigand A, Pascual-Leone A, Fox MD. Identification of Personalized

883 Transcranial Magnetic Stimulation Targets Based on Subgenual Cingulate Connectivity: An
884 Independent Replication. *Biol Psychiatry* 2021; **90**(10): e55-e6.
885 41. Fox MD, Liu H, Pascual-Leone A. Identification of reproducible individualized targets for
886 treatment of depression with TMS based on intrinsic connectivity. *Neuroimage* 2013; **66**:
887 151-60.
888 42. Gordon EM, Nelson SM. Three types of individual variation in brain networks revealed
889 by single-subject functional connectivity analyses. *Current Opinion in Behavioral Sciences*
890 2021; **40**: 79-86.
891 43. Doucet GE, Lee WH, Frangou S. Evaluation of the spatial variability in the major
892 resting-state networks across human brain functional atlases. *Hum Brain Mapp* 2019; **40**(15):
893 4577-87.
894 44. Cash RFH, Cocchi L, Lv J, Wu Y, Fitzgerald PB, Zalesky A. Personalized connectivity-guided
895 DLPFC-TMS for depression: Advancing computational feasibility, precision and reproducibility.
896 *Hum Brain Mapp* 2021.
897 45. Cole EJ, Phillips AL, Bentzley BS, et al. Stanford Neuromodulation Therapy (SNT): A
898 Double-Blind Randomized Controlled Trial. *Am J Psychiatry* 2021: appiajp202120101429.
899 46. Cole EJ, Stimpson KH, Bentzley BS, et al. Stanford Accelerated Intelligent
900 Neuromodulation Therapy for Treatment-Resistant Depression. *Am J Psychiatry* 2020; **177**(8):
901 716-26.
902 47. Williams NR, Sudheimer KD, Bentzley BS, et al. High-dose spaced theta-burst TMS as a
903 rapid-acting antidepressant in highly refractory depression. *Brain* 2018; **141**(3): e18.
904 48. Cash RFH, Zalesky A, Thomson RH, Tian Y, Cocchi L, Fitzgerald PB. Subgenual Functional
905 Connectivity Predicts Antidepressant Treatment Response to Transcranial Magnetic
906 Stimulation: Independent Validation and Evaluation of Personalization. *Biol Psychiatry* 2019;
907 **86**(2): e5-e7.
908 49. Cash RFH, Cocchi L, Lv J, Wu Y, Fitzgerald PB, Zalesky A. Personalized connectivity-guided
909 DLPFC-TMS for depression: Advancing computational feasibility, precision and reproducibility.
910 *Hum Brain Mapp* 2021; **42**(13): 4155-72.
911 50. Ojemann JG, Akbudak E, Snyder AZ, McKinstry RC, Raichle ME, Conturo TE. Anatomic
912 localization and quantitative analysis of gradient refocused echo-planar fMRI susceptibility
913 artifacts. *Neuroimage* 1997; **6**(3): 156-67.
914 51. Beckmann CF, Mackay CE, Filippini N, Smith SM. Group comparison of resting-state FMRI
915 data using multi-subject ICA and dual regression. *NeuroImage* 2009; **47**.
916 52. Zuo XN, Kelly C, Adelstein JS, Klein DF, Castellanos FX, Milham MP. Reliable intrinsic
917 connectivity networks: test-retest evaluation using ICA and dual regression approach.
918 *Neuroimage* 2010; **49**(3): 2163-77.
919 53. Li B, Zhao N, Tang N, et al. Targeting suicidal ideation in major depressive disorder with
920 MRI-navigated Stanford accelerated intelligent neuromodulation therapy. *Transl Psychiatry*
921 2024; **14**(1): 21.
922 54. Garza-Villarreal EA, Alcala-Lozano R, Fernandez-Lozano S, et al. Clinical and Functional
923 Connectivity Outcomes of 5-Hz Repetitive Transcranial Magnetic Stimulation as an Add-on
924 Treatment in Cocaine Use Disorder: A Double-Blind Randomized Controlled Trial. *Biological*
925 *psychiatry Cognitive neuroscience and neuroimaging* 2021; **6**(7): 745-57.

55. R Core Team. R: A language and environment for statistical computing. Vienna, Austria: Vienna: R Foundation for Statistical Computing; 2013.
56. Champely S, Ekstrom C, Dalgaard P, et al. pwr: Basic functions for power analysis. 2017.
57. Yan C-G, Wang X-D, Zuo X-N, Zang Y-F. DPABI: Data Processing & Analysis for (Resting-State) Brain Imaging. *Neuroinformatics* 2016; **14**(3): 339-51.
58. Yan C-G, Zang Y-F. DPARSF: A MATLAB Toolbox for "Pipeline" Data Analysis of Resting-State fMRI. *Frontiers in systems neuroscience* 2010; **4**: 13.
59. Liston C, Chen AC, Zebley BD, et al. Default mode network mechanisms of transcranial magnetic stimulation in depression. *Biol Psychiatry* 2014; **76**(7): 517-26.
60. Johnson WE, Li C, Rabinovic A. Adjusting batch effects in microarray expression data using empirical Bayes methods. *Biostatistics* 2007; **8**(1): 118-27.
61. Schaefer A, Kong R, Gordon EM, et al. Local-Global Parcellation of the Human Cerebral Cortex from Intrinsic Functional Connectivity MRI. *Cerebral cortex (New York, NY : 1991)* 2018; **28**(9): 3095-114.
62. Greicius M. Resting-state functional connectivity in neuropsychiatric disorders. *Current opinion in neurology* 2008; **21**(4): 424-30.
63. Cullen KR, Gee DG, Klimes-Dougan B, et al. A preliminary study of functional connectivity in comorbid adolescent depression. *Neuroscience Letters* 2009; **460**(3): 227-31.
64. Strikwerda-Brown C, Davey CG, Whittle S, et al. Mapping the relationship between subgenual cingulate cortex functional connectivity and depressive symptoms across adolescence. *Social cognitive and affective neuroscience* 2015; **10**(7): 961-8.
65. Ioannidis JPA. Why Most Published Research Findings Are False. *PLOS Medicine* 2005; **2**(8): e124.
66. Chen X, Lu B, Yan CG. Reproducibility of R-fMRI metrics on the impact of different strategies for multiple comparison correction and sample sizes. *Hum Brain Mapp* 2018; **39**(1): 300-18.
67. Price JL, Drevets WC. Neurocircuitry of mood disorders. *Neuropsychopharmacology* 2010; **35**(1): 192-216.
68. Price JL, Drevets WC. Neural circuits underlying the pathophysiology of mood disorders. *Trends Cogn Sci* 2012; **16**(1): 61-71.
69. Hamilton JP, Farmer M, Fogelman P, Gotlib IH. Depressive Rumination, the Default-Mode Network, and the Dark Matter of Clinical Neuroscience. *Biol Psychiatry* 2015; **78**(4): 224-30.
70. Parker G, Chan B, Hadzi-Pavlovic D. Lower rates of depression in westernised Chinese in the US. *J Affect Disord* 2007; **104**(1-3): 175-8.
71. Parker G, Gladstone G, Chee KT. Depression in the planet's largest ethnic group: the Chinese. *Am J Psychiatry* 2001; **158**(6): 857-64.
72. Qiu P, Caine ED, Hou F, Cerulli C, Wittink MN. Depression as seen through the eyes of rural Chinese women: Implications for help-seeking and the future of mental health care in China. *J Affect Disord* 2018; **227**: 38-47.
73. Kiyohara C, Yoshimasu K. Association between major depressive disorder and a functional polymorphism of the 5-hydroxytryptamine (serotonin) transporter gene: a meta-analysis. *Psychiatr Genet* 2010; **20**(2): 49-58.
74. Tagliazucchi E, Laufs H. Decoding wakefulness levels from typical fMRI resting-state data

969 reveals reliable drifts between wakefulness and sleep. *Neuron* 2014; **82**(3): 695-708.
970 75. Fitzgerald PB, Oxley TJ, Laird AR, Kulkarni J, Egan GF, Daskalakis ZJ. An analysis of
971 functional neuroimaging studies of dorsolateral prefrontal cortical activity in depression.
972 *Psychiatry Res* 2006; **148**(1): 33-45.
973 76. Rajkowska G, Goldman-Rakic PS. Cytoarchitectonic definition of prefrontal areas in the
974 normal human cortex: II. Variability in locations of areas 9 and 46 and relationship to the
975 Talairach Coordinate System. *Cerebral cortex (New York, NY : 1991)* 1995; **5**(4): 323-37.
976 77. Johnson KA, Baig M, Ramsey D, et al. Prefrontal rTMS for treating depression: location
977 and intensity results from the OPT-TMS multi-site clinical trial. *Brain Stimul* 2013; **6**(2):
978 108-17.
979 78. Perera T, George MS, Grammer G, Janicak PG, Pascual-Leone A, Wirecki TS. The Clinical
980 TMS Society Consensus Review and Treatment Recommendations for TMS Therapy for Major
981 Depressive Disorder. *Brain Stimul* 2016; **9**(3): 336-46.
982 79. Fitzgerald PB, Hoy K, McQueen S, et al. A randomized trial of rTMS targeted with MRI
983 based neuro-navigation in treatment-resistant depression. *Neuropsychopharmacology* 2009;
984 **34**(5): 1255-62.
985 80. Hebel T, Göllnitz A, Schoisswohl S, et al. A direct comparison of neuronavigated and
986 non-neuronavigated intermittent theta burst stimulation in the treatment of depression.
987 *Brain Stimul* 2021; **14**(2): 335-43.
988 81. Modak A, Fitzgerald PB. Personalising transcranial magnetic stimulation for depression
989 using neuroimaging: A systematic review. *The World Journal of Biological Psychiatry* 2021;
990 **22**(9): 647-69.
991 82. Dubois J, Adolphs R. Building a Science of Individual Differences from fMRI. *Trends in*
992 *Cognitive Sciences* 2016; **20**(6): 425-43.
993 83. Zuo XN, Xing XX. Test-retest reliabilities of resting-state FMRI measurements in human
994 brain functional connectomics: a systems neuroscience perspective. *Neurosci Biobehav Rev*
995 2014; **45**: 100-18.
996 84. Zald DH, Rauch S. The orbitofrontal cortex: Oxford University Press, USA; 2006.
997 85. Siddiqi SH, Trapp NT, Hacker CD, et al. Repetitive Transcranial Magnetic Stimulation with
998 Resting-State Network Targeting for Treatment-Resistant Depression in Traumatic Brain Injury:
999 A Randomized, Controlled, Double-Blinded Pilot Study. *J Neurotrauma* 2019; **36**(8): 1361-74.
1000 86. Schmaal L, Hibar DP, Samann PG, et al. Cortical abnormalities in adults and adolescents
1001 with major depression based on brain scans from 20 cohorts worldwide in the ENIGMA
1002 Major Depressive Disorder Working Group. *Mol Psychiatry* 2016.
1003 87. Schmaal L, Veltman DJ, van Erp TG, et al. Subcortical brain alterations in major
1004 depressive disorder: findings from the ENIGMA Major Depressive Disorder working group.
1005 *Mol Psychiatry* 2016; **21**(6): 806-12.
1006 88. Esteban O, Markiewicz CJ, Blair RW, et al. fMRIPrep: a robust preprocessing pipeline for
1007 functional MRI. *Nat Methods* 2019; **16**(1): 111-6.
1008 89. Lynch CJ, Elbau IG, Ng TH, et al. Automated optimization of TMS coil placement for
1009 personalized functional network engagement. *Neuron* 2022; **110**(20): 3263-77.e4.
1010 90. Downar J, Daskalakis ZJ. New targets for rTMS in depression: a review of convergent
1011 evidence. *Brain Stimul* 2013; **6**(3): 231-40.

1012 91. Siddiqi SH, Khosravani S, Rolston JD, Fox MD. The future of brain circuit-targeted
1013 therapeutics. *Neuropsychopharmacology* 2023.
1014 92. Dunlop K, Sheen J, Schulze L, et al. Dorsomedial prefrontal cortex repetitive transcranial
1015 magnetic stimulation for treatment-refractory major depressive disorder: A three-arm,
1016 blinded, randomized controlled trial. *Brain Stimul* 2020; **13**(2): 337-40.
1017 93. Zuo X-N, Xing X-X. Test-retest reliabilities of resting-state FMRI measurements in human
1018 brain functional connectomics: A systems neuroscience perspective. *Neuroscience &*
1019 *Biobehavioral Reviews* 2014; **45**: 100-18.
1020 94. Wang D, Buckner RL, Fox MD, et al. Parcellating cortical functional networks in
1021 individuals. *Nat Neurosci* 2015; **18**(12): 1853-60.
1022 95. Marek S, Tervo-Clemmens B, Calabro FJ, et al. Reproducible brain-wide association
1023 studies require thousands of individuals. *Nature* 2022; **603**(7902): 654-60.
1024 96. Lu B, Chen X, Xavier Castellanos F, et al. The power of many brains: Catalyzing
1025 neuropsychiatric discovery through open neuroimaging data and large-scale collaboration.
1026 *Sci Bull (Beijing)* 2024; **69**(10): 1536-55.
1027 97. Chen X, Lu B, Li HX, et al. The DIRECT consortium and the REST-meta-MDD project:
1028 towards neuroimaging biomarkers of major depressive disorder. *Psychoradiology* 2022; **2**(1):
1029 32-42.
1030 98. Wang YW, Chen X, Yan CG. Comprehensive evaluation of harmonization on functional
1031 brain imaging for multisite data-fusion. *Neuroimage* 2023: 120089.
1032

1033 Table 1. Demographic and clinical data for all samples included in the DIRECT II project

Site	Age (HC)[1]	Age (MDD)[1]	% Male (HC)[2]	% Female (HC)[2]	% Male (MDD)[2]	% Female (MDD)[2]	Education (HC, years)[1]	Education (MDD, years)[1]	Age at the onset of the first episode (years)[1]	Episode number[1]	Full episode durations (months)[1]	HAMD-17 score[1]	N (HC)	N (MDD)
1	39.33 (15.80)	38.67 (13.50)	87 (35.22%)	160 (64.78%)	98 (35.13%)	181 (64.87%)	13.05 (3.89)	12.03 (3.62)	35.75 (13.47)	1.19 (0.40)	49.01 (64.25)	20.96 (5.60)	247	279
2	20.90 (2.89)	19.02 (3.79)	24 (38.71%)	38 (61.29%)	37 (27.41%)	98 (72.59%)	13.73 (1.80)	11.97 (2.55)	16.28 (4.05)	1.07 (0.35)	16.94 (19.74)	18.06 (8.99)	62	135
3	26.50 (11.22)	34.40 (10.56)	5 (25.00%)	15 (75.00%)	5 (25.00%)	15 (75.00%)	15.40 (1.47)	14.90 (2.97)	35.55 (11.96)	1.15 (0.49)	14.50 (29.14)	29.37 (6.41)	20	20
4	29.89 (9.88)	30.87 (10.39)	9 (33.33%)	18 (66.67%)	13 (41.94%)	18 (58.06%)	13.04 (3.80)	12.65 (4.22)	26.80 (10.89)	2.52 (3.66)	42.03 (58.57)	21.79 (5.74)	27	31
5	36.79 (9.07)	33.59 (9.85)	32 (56.14%)	25 (43.86%)	60 (46.88%)	68 (53.13%)	14.37 (2.64)	13.07 (3.43)	NA	1.00 (0.00)	NA	26.59 (3.76)	57	128
6	23.75 (5.15)	30.90 (9.29)	45 (44.55%)	56 (55.45%)	31 (52.54%)	28 (47.46%)	13.88 (2.31)	12.03 (3.06)	28.14 (9.46)	1.87 (1.12)	44.14 (61.28)	20.51 (6.71)	101	59
7	19.80 (3.85)	20.00 (6.51)	8 (26.67%)	22 (73.33%)	5 (23.81%)	16 (76.19%)	11.90 (2.55)	10.81 (2.86)	18.81 (7.19)	1.10 (0.30)	15.60 (16.23)	24.10 (12.68)	30	21
8	31.93 (9.66)	32.84 (8.95)	18 (42.86%)	24 (57.14%)	15 (34.88%)	28 (65.12%)	15.40 (1.86)	15.79 (1.82)	30.60 (8.78)	3.65 (2.29)	21.51 (11.65)	23.84 (3.88)	42	43
9	36.12 (13.85)	45.11 (14.32)	10 (40.00%)	15 (60.00%)	19 (40.43%)	28 (59.57%)	13.56 (4.01)	10.83 (4.52)	42.19 (14.23)	1.43 (0.77)	36.07 (53.22)	NA	25	47

10	36.49 (12.64)	34.00 (11.81)	30 (44.78%)	37 (55.22%)	36 (45.00%)	44 (55.00%)	14.58 (2.30)	13.25 (3.08)	26.15 (10.47)	2.30 (1.78)	92.00 (96.70)	14.58 (8.21)	67	80
11	36.62 (12.11)	38.29 (12.75)	30 (44.12%)	38 (55.88%)	55 (48.67%)	58 (51.33%)	12.96 (3.57)	10.96 (3.48)	32.21 (12.46)	3.36 (3.63)	75.51 (93.37)	23.54 (9.23)	68	113
12	29.59 (5.00)	30.47 (7.20)	15 (46.88%)	17 (53.13%)	21 (33.87%)	41 (66.13%)	14.59 (2.82)	13.73 (3.39)	29.63 (7.11)	1.00 (0.00)	6.10 (4.22)	21.27 (3.47)	32	62
13	35.45 (13.76)	38.00 (14.56)	9 (31.03%)	20 (68.97%)	13 (40.63%)	19 (59.38%)	11.28 (4.31)	12.03 (3.87)	33.09 (13.93)	1.45 (1.12)	NA	18.66 (9.66)	29	32
14	38.10 (11.96)	43.50 (11.28)	65 (45.14%)	79 (54.86%)	47 (34.56%)	89 (65.44%)	13.24 (4.20)	9.07 (3.60)	37.52 (11.50)	2.55 (2.15)	67.16 (77.29)	30.04 (10.52)	144	136
15	21.51 (4.58)	22.06 (4.70)	23 (65.71%)	12 (34.29%)	7 (20.59%)	27 (79.41%)	12.57 (1.42)	11.85 (2.39)	21.82 (5.19)	2.50 (2.81)	12.76 (15.11)	NA	35	34
16	25.73 (7.38)	26.07 (7.66)	44 (54.32%)	37 (45.68%)	37 (44.58%)	46 (55.42%)	15.53 (2.81)	13.81 (2.60)	23.02 (8.11)	1.73 (1.11)	30.18 (44.24)	25.42 (3.78)	81	83
17	34.73 (9.66)	35.21 (9.43)	19 (38.78%)	30 (61.22%)	15 (35.71%)	27 (64.29%)	14.31 (4.21)	12.50 (4.09)	35.00 (9.53)	1.00 (0.00)	3.79 (2.62)	23.67 (5.25)	49	42
18	32.19 (11.83)	35.25 (13.15)	13 (40.63%)	19 (59.38%)	12 (50.00%)	12 (50.00%)	12.53 (3.03)	13.42 (4.47)	NA	1.58 (0.72)	17.77 (19.57)	22.38 (4.23)	32	24
19	30.94 (7.32)	27.03 (11.04)	16 (50.00%)	16 (50.00%)	5 (15.63%)	27 (84.38%)	13.94 (2.84)	12.69 (3.18)	25.58 (10.86)	1.28 (0.46)	12.88 (14.38)	23.06 (5.66)	32	32
20	31.40 (10.99)	27.80 (8.99)	5 (25.00%)	15 (75.00%)	4 (20.00%)	16 (80.00%)	16.10 (3.21)	13.60 (4.36)	26.65 (9.21)	1.30 (0.47)	14.55 (15.14)	24.85 (6.47)	20	20
21	32.80 (11.06)	32.52 (11.44)	31 (55.36%)	25 (44.64%)	17 (28.33%)	43 (71.67%)	15.88 (4.59)	12.20 (4.12)	31.44 (11.70)	NaN (NaN)	35.79 (44.90)	22.71 (2.62)	56	60
22	34.67 (13.54)	35.74 (10.02)	8 (33.33%)	16 (66.67%)	10 (28.57%)	25 (71.43%)	14.21 (2.86)	13.20 (3.75)	31.23 (7.91)	1.06 (1.35)	5.59 (14.93)	22.29 (6.04)	24	35

23	13.57 (2.18)	13.91 (1.48)	14 (50.00%)	14 (50.00%)	8 (13.79%)	50 (86.21%)	7.57 (2.18)	7.91 (1.48)	NA	NA	NA	NA	28	58

1 Mean (SD)

2 N (%)

NA: data were missing for this site.